A compositional kinetic model of hydrate crystallization and dissolution

Lawrence M. Cathles[1]

Department of Earth and Atmospheric Sciences, Cornell University, Ithaca, New York, USA

Duo Fu Chen[2]

Key Laboratory of Marginal Sea Geology, Guangzhou Institute of Geochemistry and South China Sea Institute of Oceanology, Chinese Academy of Sciences, Wushan, China

Received 25 November 2003; revised 15 May 2004; accepted 9 June 2004; published 10 August 2004.

[1] Hydrates are crystallizing near and at the seafloor from gas vents on shelves where the sedimentation rate is high and hydrocarbons are being generated. When seafloor temperature, vent rate, or vent gas composition changes, these hydrates may become unstable and decompose. We have constructed a compositional kinetic model of hydrate crystallization and dissolution that can address these issues. The model crystallizes hydrate in compositional bins and allows each to dissolve at either a kinetically or compositionally controlled rate if vent gas composition or temperature causes it to become unstable. We empirically calibrate the model to venting at the Bush Hill hydrate mound in the offshore Louisiana Gulf of Mexico, show how variations in venting rate crystallize hydrate of diverse composition in the subsurface, and investigate how bottom water temperature variations similar to those measured could increase the rate of gas venting by destabilizing hydrates within a few meters of the seafloor. We show that increases in bottom water temperature can cause gas venting rates to increase ~100%, as suggested by recent measurements, only if the dissolution kinetics are fast compared to the empirically calibrated crystallization kinetics and dissolution gases are removed rapidly enough that they do not thermodynamically inhibit the rate of dissolution. Model characteristics required to further investigate hydrate mound construction are identified. *INDEX TERMS:* 1050 Geochemistry: Marine geochemistry (4835, 4850); 1045 Geochemistry: Low-temperature geochemistry; 1055 Geochemistry: Organic geochemistry; 1030 Geochemistry: Geochemical cycles (0330); 1635 Global Change: Oceans (4203); *KEYWORDS:* compositional kinetic model, gas venting, hydrate crystallization, dissolution, methane, seafloor seep

Citation: Cathles, L. M., and D. F. Chen (2004), A compositional kinetic model of hydrate crystallization and dissolution, *J. Geophys. Res.*, *109*, B08102, doi:10.1029/2003JB002910.

1. Introduction

[2] Gas hydrate is an ice-like crystalline mineral in which a rigid cage of water molecules encloses hydrocarbon and nonhydrocarbon gas molecules [*Sloan*, 1998]. Recent research has shown that gas hydrates are extremely common over vast areas of the world's shelves and continental slopes and in arctic permafrost. Hydrates may contain 10^{19} g [*Kvenvolden and Lorenson*, 2001] of mostly methane carbon and thus represent a gas resource as large as all the fossil fuels combined. For this reason, hydrates are today a very active area of hydrocarbon research.

[3] Two end-member types of hydrate accumulation occur in nature. The first, which undoubtedly characterizes the greatest number of hydrate occurrences, occurs in areas of very slow sedimentation and gas leakage. The gas flux is low relative to the vertical water flux, and a gap separates the base of the hydrate stability layer from seismically reflective free gas that produces the bottom simulating reflector (BSR) at these hydrate occurrences [e.g., *Hyndman and Davis*, 1992; *Dickens and Quinby-Hunt*, 1997]. No free gas occurs in the hydrate stability zone, and the diffusion of methane dissolved in the pore water dissolves hydrate near the seafloor, producing a hydrate-free gap between the shallowest occurrence of hydrate and the seafloor. The width of both gaps provides a measure of the gas flux at the site. Hydrate accumulation can be modeled using heat and mass balance only; the kinetics of hydrate crystallization need not be considered [*Xu and Ruppel*, 1999; *Rempel and Buffett*, 1997].

[4] The other end-member type of hydrate occurrence is found in fault zones bordering salt domes in the offshore

[1] Also at Key Laboratory of Marginal Sea Geology, Guangzhou Institute of Geochemistry and South China Sea Institute of Oceanology, Chinese Academy of Sciences, Wushan, China.

[2] Also at Gas Hydrate Research Center, Chinese Academy of Sciences, Wushan, China.

0148-0227/04/2003JB002910$09.00

Gulf of Mexico. Bush Hill in Green Canyon Block 184 off the Louisiana coast is perhaps the type example. At these sites, hydrate presumably is present from the base of hydrate stability to the seafloor, and gas actively vents through the entire hydrate stability zone and bubbles into the overlying ocean. This type of hydrate accumulation requires consideration of the kinetics of hydrate crystallization from a gas stream. In this paper we extend models that we have developed to include the composition of crystallized hydrate, hydrate dissolution caused by changes in vent gas chemistry, and hydrate dissolution caused by changes in bottom water temperature. In what follows, we first review our models and describe the compositional kinetic model we have developed. We then use this model to analyze selected aspects of the Bush Hill system.

2. Hydrate Models and Observations at Bush Hill

[5] *Chen and Cathles* [2003] developed the first kinetic model for the crystallization of hydrate from a gas stream and applied it to the Bush Hill vent site. They showed that the gas venting at Bush Hill would have the observed average composition if ~9% of a gas with the average compositions of that in producing reservoirs [*Sassen et al.*, 2001a] in the fault system connected to the vent was precipitated as hydrate in the Bush Hill hydrate mound. The predicted profile of hydrate crystallization was used to project the surface exposure of the mound into the subsurface. Assuming that the mound contained an average 2 vol % hydrate, about the same volume of methane (~0.8 Mt) is contained in subsurface hydrates at Bush Hill as in the Jolliet gas reservoirs that lie deeper in the vent fault system. If this hydrate accumulated over the last ~10,000 years, as seems geologically reasonable, and if present conditions applied in the past, methane has been venting at the rate of ~800 t yr^{-1} from the mound over this period. Chen and Cathles also showed that variations in vent and hydrate chemistry could be caused by variations in gas venting rate.

[6] *Chen et al.* [2004] further investigated the evidence for variations in venting rate at Bush Hill. They compiled observational data suggesting that at any instant of time, gas is venting to the surface through a number of channels at very different rates. The difference in venting rates in individual channels produces a range in vent gas and hydrate composition that is nearly as large as can be produced by hydrate crystallization. The channel venting rate ranges from rates so slow that nearly all the higher (C_{2+}) hydrocarbon components crystallized as hydrates to rates so fast that only a very small fraction of these components is removed. Changes in vent gas composition between repeat submersible visits to the same site (possibly the same channel) suggest that the vent gas composition at each channel is also changing with time. The fact the vent gases appear wetter (more enriched in $C_3 + C_4$) than expected on the basis of the $C_3 + C_4$ content of the hydrates sampled from the mound indicates that the local rate of gas venting may be increasing with time. This could occur in a waning vent system if the venting is progressively organized into fewer, faster moving channels as the system ages.

[7] The analyses of both *Chen and Cathles* [2003] and *Chen et al.* [2004] are static. The gas venting rate is assumed to be constant, the subsurface temperature field is assumed not to change, and only hydrate crystallization is modeled. The pattern of hydrate crystallization and its effect on vent gas composition are calculated for a series of constant venting rates and subsurface thermal gradients to reach the conclusions just summarized.

[8] This paper extends the previous model by keeping track of the composition of the hydrate crystallized and by allowing hydrate to dissolve as well as crystallize. The extended model is used here to investigate how observed variations in venting rate that occur when bottom water temperature rises could be related to the dissolution of near-surface hydrate. Our analysis shows that for the gas venting rates to change with bottom water temperature as observed, the dissolution kinetics in our model must be much faster than the crystallization kinetics and the dissolved gas must not inhibit the dissolution reaction. If the dissolution kinetics are this fast, hydrate should significantly dissolve from the mound interior when venting rates drop.

[9] The data set that motivates the model developed in this paper is shown in Figure 1. Venting rates were measured at one Bush Hill vent site with a Savonius rotor for about a 1 month period, and bottom water temperatures were measured at the same time. The equipment and procedures are fully described by *Roberts et al.* [1999]. As shown in Figure 1, the ~30 day record shows marked changes in gas venting rate. Positive excursions in the venting rate exhibit a decreasing correlation with temperature over time. For example, the first increase in venting rate (at ~2 days) correlates with a strong spike in bottom water temperature. A broad increase in bottom water temperature starting at ~15 days correlates with a broad (but smaller) increase in gas emission rate. However, there is no increase in gas venting rate following a strong spike in bottom water temperature at ~35 days.

3. Theory

[10] As in the work by *Chen and Cathles* [2003], the model we will apply here assumes that the crystallization of gas from a stream can be described by a first-order rate equation:

$$\frac{\partial m}{\partial t} = -k\Delta X^g \exp\left[\frac{E}{R}\left(\frac{1}{T^*} - \frac{1}{T}\right)\right], \tag{1}$$

where m [kg m^{-3} yr^{-1}] is the mass of gas crystallized as hydrate, k [kg m^{-3} yr^{-1}] is the rate constant, ΔX^g is the difference ($X^g - X_f^{g-eq}$) between mass fraction $C_3 + C_4$ in the gas stream, X^g, and the fictive (subscript f) mass fraction $C_3 + C_4$ in the gas that would be in equilibrium with hydrate crystallizing from this gas, X_f^{g-eq}. E^* is the activation energy of the crystallization reaction, R is the gas constant, T is temperature in °K, and T^* is a reference temperature of 273.15°K. The units of m and k are the same, and we take the units of both to be kg m^{-3} yr^{-1}. From *Chen and Cathles* [2003] we will take E^*/R = 10,000°K and define X_f^{g-eq} as a polynomial expansion in pressure and temperature on the basis of calculations using *Sloan*'s [1998] CSMHYD program. *Chen and Cathles* [2003] showed that 9% of a gas stream crystallized as hydrate at Bush Hill if a dimensionless lumped kinetic parameter $K = L_e k/q$ = 0.015 for a depth interval L_e of 60 m. Thus $k = 2.5 \times 10^{-4} q$ at Bush Hill.

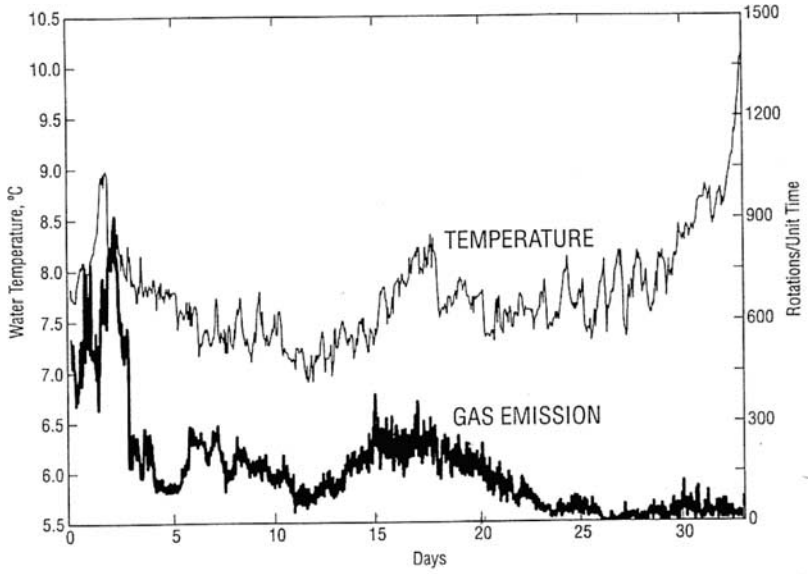

Figure 1. Bottom water temperature and total rotations in a 30 min summation period of a Savonius-type rotor positioned over the bubble stream. From *Roberts et al.* [1999] (© 1999 Offshore Technology Conference Paper OTC10770).

[11] The fraction of the gas stream that is crystallized in any depth interval, L_e [m], is

$$F_e = \frac{\Delta m}{m} = \frac{\frac{\partial m}{\partial t} L_e}{q}, \tag{2}$$

where q is the vertical gas flux into the base of L_e in kg m^{-2} yr^{-1}. The gas flux changes across L_e:

$$q[z + 0.5L_e] = q[z - 0.5L_e](1 - F_e), \tag{3}$$

where depth is positive upward. Mass balance requires that the composition of the gas stream is changed by hydrate crystallization:

$$X^g[z + 0.5L_e] = \frac{X^g[z - 0.5L_e] + F_e X^H[z - 0.5L_e]}{1 - F_e}, \tag{4}$$

where X^H is the mass fraction of $C_3 + C_4$ in the hydrate that is crystallized from the gas stream in L_e. X^H is determined from X^g and temperature by a polynomial regression defined by *Chen and Cathles* [2003]. So far, the model is exactly the same as described by *Chen and Cathles* [2003] except the rate constant is defined explicitly rather than included in a dimensionless lumped parameter.

[12] The model departs from *Chen and Cathles* [2003] at this point. The mass of gas crystallized as hydrate in depth interval L_e, m, has a composition X^H. This mass of hydrate gas is placed in a bin with a defined composition range that includes X^H. We use 22 hydrate bins (as shown in Table 1) in the modeling reported here. The driest (least $C_3 + C_4$) hydrate bin starts at $X^H = 0$ and ends at $X^H = 0.032$. The bin widths decrease by a factor of 0.95 between subsequent bins. The 21st bin start at $X^H = 0.409$ and ends at $X^H = 0.420$. The last bin is open (extending from $X^H = 0.42$ to $X^H = \infty$).

[13] Kinetically, we describe the amount of hydrate that can dissolve from bin j over time, t:

$$\Delta M_j^{\text{kin}} = kS\Delta X_j^g \exp\left[\frac{E}{R}\left(\frac{1}{T^*} - \frac{1}{T}\right)\right] L_e \Delta t, \tag{5}$$

where ΔM_j^{kin} [kg m^{-2}] is the mass of hydrate dissolved from an interval of depth, L_e, over time, t, S is a dimensionless constant that allows the dissolution kinetics to differ from the crystallization kinetics of equation (1), and $\Delta X_j^g = X^g - X_j^{g-\text{eq}H}$, where $X_j^{g-\text{eq}H}$ is the mass fraction $C_3 + C_4$ of gas in equilibrium with hydrate in bin j at the temperature in L_e, and the other variables are as defined as in equation (1). $X_j^{g-\text{eq}H}$ is determined in terms

Table 1. Hydrate Average Composition in the Bins

	Bin Boundary			
Bin	Bottom	Top	Bin Width	$\overline{X_j}$
1	0.000	0.032	0.032	0.016
2	0.032	0.062	0.030	0.047
3	0.062	0.091	0.029	0.077
4	0.091	0.118	0.027	0.105
5	0.118	0.144	0.026	0.131
6	0.144	0.169	0.025	0.157
7	0.169	0.192	0.023	0.181
8	0.192	0.214	0.022	0.203
9	0.214	0.235	0.021	0.225
10	0.235	0.256	0.021	0.246
11	0.256	0.275	0.019	0.266
12	0.275	0.293	0.018	0.284
13	0.293	0.310	0.017	0.302
14	0.310	0.326	0.016	0.318
15	0.326	0.342	0.016	0.334
16	0.342	0.357	0.015	0.350
17	0.357	0.371	0.014	0.364
18	0.371	0.384	0.013	0.378
19	0.384	0.397	0.013	0.391
20	0.397	0.409	0.012	0.403
21	0.409	0.420	0.011	0.415
22	0.420	∞	∞	>0.420

of X^g and temperature by a polynomial expansion defined by *Chen and Cathles* [2003] hydrate to be dissolved. ΔX_j^g must be less than 0. Hydrate is dissolved if $X^g < X_j^{g-\mathrm{eq}H}$s, but hydrate is not crystallized if $X^g > X_j^{g-\mathrm{eq}H}$. Crystallization is simulated by equation (1).

[14] The maximum amount of hydrate, $\Delta M_j^{\mathrm{pot}}$, in kg m^{-2} that can be dissolved over a time step from bin j over interval L_e is the amount present in bin j at the start of the time step. If G_j is the mass of hydrate in bin j per cubic meter of sediment,

$$\Delta M_j^{\mathrm{pot}} = -G_j L_e. \tag{6}$$

Finally, since by equation (5) hydrate can dissolve only so long as $\Delta X_j^g < 0$ (e.g., the gas vent stream in element e contains less $C_3 + C_4$ than would be in equilibrium with hydrate of bin j composition, $X_j^{g-\mathrm{eq}H}$), hydrate dissolution from bin j must cease when the mass of hydrate dissolved L_e rises X^g to $X_j^{g-\mathrm{eq}H}$. Mass balance of $C_3 + C_4$ input, dissolution, and efflux from L_e, q_{dissol}, defines this thermodynamic limit:

$$\mathrm{q}X_g + q_{\mathrm{dissol}} X_j^H = (q + q_{\mathrm{dissol}}) X_j^{g-\mathrm{eq}H}.$$

Since $\Delta M_j^{\mathrm{Ther\ mod}} = q_{\mathrm{dissol}}\, \Delta t$, substituting for q_{dissol} yields

$$\Delta M_j^{\mathrm{Ther\ mod}} = q\Delta t \left(\frac{X_j^{eq-H} - X^g}{X_j^H - X_j^{eq-H}} \right). \tag{7}$$

Here $\Delta M_j^{\mathrm{Ther\ mod}}$ is the amount of hydrate that can be dissolved before the gas in L_e becomes saturated with respect to bin j hydrate (e.g., the thermodynamic or equilibrium limit), and Δt is the time step of the calculation.

[15] Equations (5), (6), and (7) are used to model hydrate dissolution in the following fashion. X^g is determined from equation (4). Hydrate bins that are unstable with respect to this gas composition are then identified, and hydrate is dissolved from the wettest bin (e.g., the bin with hydrates richest in $C_3 + C_4$) first. The mass of hydrate dissolved in depth interval L_e, ΔM_j, is taken to be the minimum of the possible controlling values:

$$\Delta M_j = \min\left(\Delta M_j^{\mathrm{pot}}, \Delta M_j^{\mathrm{kin}}, \Delta M_j^{\mathrm{Ther\,mod}} \right). \tag{8}$$

The entire bin is dissolved if $\Delta M_j^{\mathrm{pot}}$ is the minimum. If kinetics limits the dissolution, $\Delta M_j^{\mathrm{kin}}$ is the minimum. The bin dissolves at the kinetic rate without exhausting the hydrate in bin j. If the dissolution of hydrate brings the vent gas into equilibrium with bin j hydrate and causes the dissolution to stop, $\Delta M_j^{\mathrm{Ther\ mod}}$ is the minimum. In this case, only enough hydrate is dissolved from bin j to saturate the gas stream with respect to bin j. The dissolution of the next wettest bin is computed in the same fashion. This continues until all the disequilibrium hydrate bins have been considered or until the gas stream is brought into thermodynamic equilibrium with all undissolved hydrate bins. Kinetics can be increased by taking $S > 1$. Infinite kinetics can be simulated if $\Delta M_j^{\mathrm{kin}}$ is dropped from the list in equation (8).

[16] At each dissolution step, a fraction of gas, F_j, is added to the gas stream:

$$F_j = \frac{\Delta M_j}{q\Delta t}, \tag{9}$$

the composition of the gas stream is modified

$$X_{t+1}^g = \frac{F_j X_j^H + X_t^g}{F_j + 1}, \tag{10}$$

and the gas mass flux is modified

$$q_{t+1} = q_t + \frac{\Delta M_j}{\Delta t}. \tag{11}$$

In equations (10) and (11) the variable on the left is the updated (by dissolution of bin j hydrate) version of the variable on the right. This is indicated by subscript $t + 1$ and t, respectively.

[17] The gas composition and hydrate crystallization/dissolution profiles are computed in propagator fashion, starting at the base of the hydrate stability zone as described by *Chen and Cathles* [2003]. Hydrate stability depends on temperature, pressure, and gas composition [*Sloan*, 1998; *Chen and Cathles*, 2003]. We model temperature changes due to sedimentation, changes in heat flow, and changes in surface temperature by solving the transient one-dimensional conservation of heat equation in a coordinate system attached to the sediment grains using standard finite element techniques [*Baker and Pepper*, 1991]. The solution equation is

$$\rho_m c_m \frac{DT}{Dt} = \frac{\partial}{\partial z} K[\phi, T, S_H] \frac{\partial T}{\partial z}, \tag{12}$$

where $\rho_m c_m$ is the heat capacity per unit volume of the sediments (taken to be a constant equal to 0.55 cal cm^{-3} °C^{-1}), and K is the thermal conductivity of the sediments as a function of porosity, ϕ, temperature, T, and hydrate pore fraction, S_H. At each time step the temperature of the top boundary is set at T_s. T_s may change with time (e.g., have a different value at different time steps in the solution). A Neumann condition of constant heat flow is applied at the bottom boundary at each time step; the heat flow can change between time steps. To allow simulation of the shallow subsurface temperature changes produced by rapid (days to months) changes in bottom water temperature, the subsurface is discretized in intervals that exponentially increase with depth up to some thickness where the intervals are thereafter of constant thickness. The uppermost layer might be centimeters thick, and the constant thickness lowermost layers may be tens of meters thick, for example. These initial, exponentially increasing layer thicknesses are then compacted as actual sediment layers would be. The compacted thicknesses and the corresponding diminished porosities are used in the thermal calculations.

[18] Porosity is assumed to be a liner function of effective stress, σ_{eff}, to a minimum porosity of ~10% (which is not

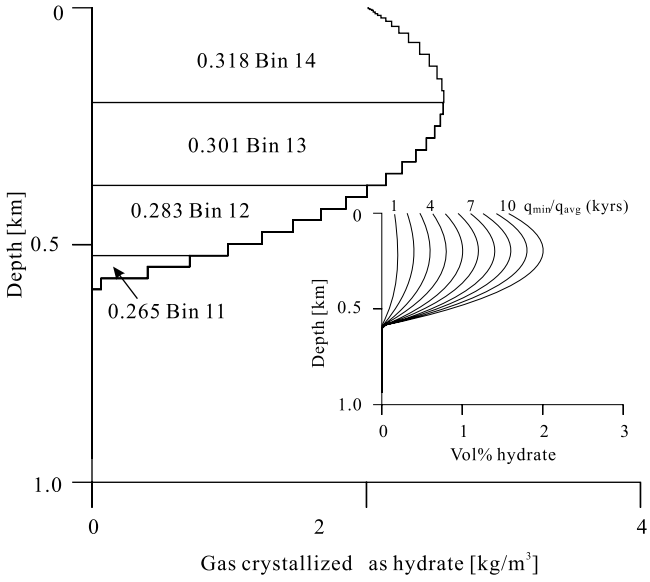

Figure 2. Calculated hydrate composition in a local vent discharging gas at a constant rate such that the kinetic rate constant $k = 2.5 \times 10^{-4}$ q_{avg} kg m^{-3} yr^{-1} and the feed gas entering the base of the hydrate stability zone has X^g = 0.047. Compositional bin numbers and the average mass fraction $C_3 + C_4$ in hydrate in these bins are shown. The insert shows that ~2 vol % hydrate will accumulate throughout the hydrate stability field in 10,000 years times q_{avg}/q_{min}, where q_{min} is the minimum gas flux obtained if venting occurs uniformly through the Bush Hill hydrate mound at the inferred rate (see text discussion) and q_{avg} is average gas flux through the mound that affects the chemistry of a particular bubble stream.

reached in the depth interval we consider in this paper). Above the minimum,

$$d\phi = -\phi_o \beta \, d\sigma_{\text{eff}},$$

$$d\sigma_{\text{eff}} = (1 - \phi_o)(\rho_G - \rho_w) g z_u, \qquad (13)$$

$$\Delta z = \Delta z_u \frac{1 - \phi_o}{1 - \bar{\phi}},$$

where β is the long-term sediment compressibility, ϕ_o is the sediment porosity at the surface, g is the gravitational acceleration, ρ_G is the density of the sediment mineral grains, ρ_w is the density of the pore water, z_u is the depth to the boundaries of the uncompacted (initial) sediment layers, Δz is the thickness of a compacted layer, Δz_u is the thickness of the uncompacted layer, and $\bar{\phi}$ is the average porosity of that layer. We use $\phi_o = 0.35$ and $\beta = 6.136 \times 10^{-4}$ bar^{-1}. These values are suitable for compaction of shale in the offshore Louisiana Gulf Coast [cf. *Revil and Cathles*, 2002].

[19] Thermal conductivity is defined in our model as a function of porosity, temperature, and the hydrate pore fraction using a fabric theory approach described by *Luo et al.* [1994]. This model allows temperature-dependent thermal conductivities of shale, water, and hydrate to be separately defined and properly combined to simulate the thermal conductivity of a water-saturated porous sediment whose pores are partially filled with hydrate. If hydrate has a thermal conductivity similar to gas, its crystallization in sediment pores could significantly affect the thermal conductivity of the sediment, and these changes could affect temperatures in a hydrate mound significantly. In the calculations presented here we do not include the thermal conductivity effect of hydrate pore filling. We take the thermal conductivity of hydrate to be that of water. We do not consider the thermal effects of hydrate crystallization and dissolution. We also assume that heat advection by gas venting does not perturb the subsurface temperature profile. All of these effects can be important under certain circumstances, and we delineate what these circumstances are in section 5. We will consider these effects in a future paper. They do not affect the conclusions reported here.

4. Analysis of Phenomena at the Bush Hill Gas Vent/Hydrate Mound

[20] The compositional model just described allows us to calculate the subsurface composition of hydrates in a mound. If the venting rate is constant, the results are particularly simple. Figure 2 shows the composition of hydrate that crystallizes in the subsurface if the venting rate is constant. For steady venting, the composition of the hydrate crystallized depends only on temperature and pressure, and the $C_3 + C_4$ composition of the hydrate is greater near the surface than at depth.

[21] The Figure 2 insert shows how hydrate will accumulate with time. We express this accumulation time in a fashion that accommodates different venting rates by multiplying the time axis by q_{min}/q_{avg}. Thus, for example, if $q_{min}/q_{avg} = 0.5$, 2 vol % hydrate will accumulate in 5000 years rather than 10,000 years. The hydrate accumulates faster because we assume that the crystallization rate constant is proportional to the gas mass flux (e.g., k [m^{-1}] = $0.00025 q_{avg}$) so the model system operates as we have inferred [*Chen and Cathles*, 2003] that the Bush Hill system is operating at the higher gas flux. For example, 9% of the venting gas crystallizes in the mound and shifts the vent gas from the source composition as observed (see discussion following equation (1)). The gas flux through the mound will be increased if the gas moves through a set of pipe-like channels whose aggregate plan area is less than the plan area of the mound, for example. Thus we define a minimum gas flux equal to that which would pertain if the gas moved uniformly through the whole mound ($q_{min} \sim 1.6$ kg m^{-2} yr = 800×10^3 kg yr^{-1} divided by the area of the 800 m diameter mound) and allow the actual average gas flux, q_{avg}, to differ from this minimum value. The ratio of q_{min}/q_{avg} might reflect the ratio of channel to the mound plan areas, although q_{avg} could also differ from q_{min} for other reasons (such as if we had overestimated or underestimated the rate of venting at Bush Hill because the time of accumulation was not 10,000 years or because the mound contains some different volume percent hydrate, or because the mound does not extend as deeply, etc.).

[22] Crystallization of more varied hydrate compositions will occur if the rate of gas venting changes with time about its mean venting rate, q_{avg}. This is illustrated in Figure 3 for a case where the q/q_{avg} increases from 0.25 to 1.9325 in

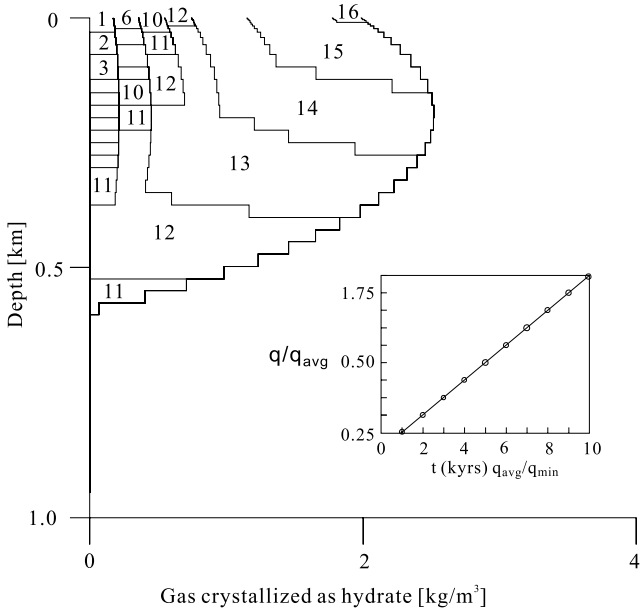

Figure 3. Composition of hydrate crystallized as a function of depth when gas mass flux, q, increases from $0.25q_{avg}$ to $1.9325q_{avg}$ in steps of $0.1875q_{avg}$. The initial slow venting crystallizes hydrate with $C_3 + C_4$ compositions less than or equal to those in bin 12. The later fast venting deposits hydrate wetter (more enriched in $C_3 + C_4$) than the hydrate in bin 11. Vertical deposition bands demarcate the 10 time steps with their different gas fluxes, q. Hydrate bin numbers are given in Table 1. Figure 4 shows the hydrate and vent gas composition profiles at the 10 venting rates.

nine steps of 0.1875. The average venting rate remains q_{avg} for this sequence of venting rates. The $C_3 + C_4$ content of the hydrate deposited from the gas stream changes with time, however, because the gas becomes richer in $C_3 + C_4$ as the venting rate increases. Figure 4 shows depth profiles of the gas composition and the hydrate that is crystallizing from it at the venting rates imposed over the time period of the simulation. At early times when the venting rate is slow, the gas stream becomes depleted in $C_3 + C_4$, and the hydrate crystallized near the surface is lean in $C_3 + C_4$ (occupies the low number hydrate bins). At the end of the simulation, when the venting rate is fast, the gas stream is richer in $C_3 + C_4$, and the hydrates are deposited in higher number bins richer in $C_3 + C_4$. The 10 venting rates are reflected compositionally in Figure 3 by the roughly vertical boundaries between bin numbers. The earliest crystallized hydrate is the band of bins on the left.

[23] Cycling the venting rate up and then down produces a still more complex pattern of subsurface hydrate composition because hydrate rich in $C_3 + C_4$ that is crystallized at the fast venting rates will dissolve when exposed to the dry vent gas compositions of the later slow venting rates. The hydrates rich in $C_3 + C_4$ are unstable with respect to the lean gas stream. The subsurface hydrate compositions are not very strongly affected if the dissolution rate constant is the same as for crystallization but can be dramatic if the dissolution kinetics are fast.

[24] Figures 5 and 6 show the profiles of subsurface hydrate composition that results if the venting rate is first increased from 0.25 to 1.9325 in nine steps of 0.1875 and then decreases in the same fashion. The average venting rate remains q_{avg}. Figure 5 shows how the hydrate accumulates and dissolves if the dissolution kinetics are the same as for crystallization (e.g., $S = 1$, k [kg m^{-3} yr^{-1}] = $2.5 \times 10^{-4} q_{avg}$). The pattern is not much changed from the case where the venting rate only increased and there was no dissolution (Figure 3). Figure 6 shows that dissolution has a substantial impact if the dissolution kinetics are infinitely fast. Bands of dissolution occur at ~120, 250, and 400 m depth.

[25] The bands of hydrate dissolution can be understood as follows: Crystallization and dissolution in each element in the spatially discretized vertical path from the base of the hydrate stability zone to the surface are evaluated sequentially by our propagator method of solution, starting at the base and working upward. Because hydrate is strongly enriched in $C_3 + C_4$, the amount of hydrate that must be dissolved to bring the gas in an element into equilibrium

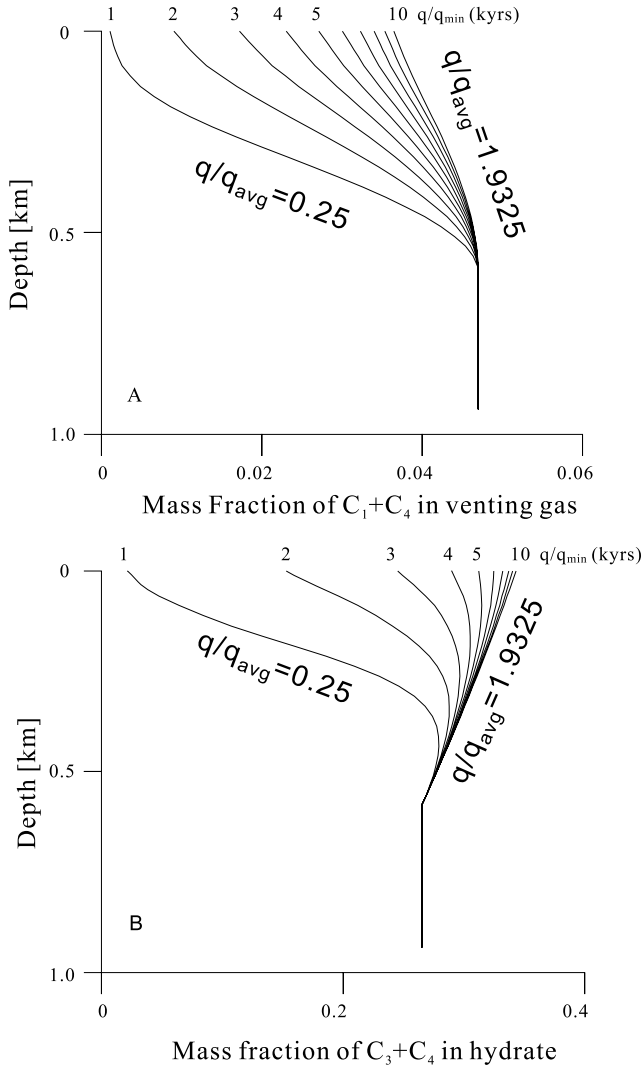

Figure 4. (a) Depth profiles of the mass fraction $C_3 + C_4$ in vent gas for the venting rate in Figure 3. (b) Depth profile of the mass fraction of $C_3 + C_4$ in hydrate crystallizing at various times for the case shown in Figure 3.

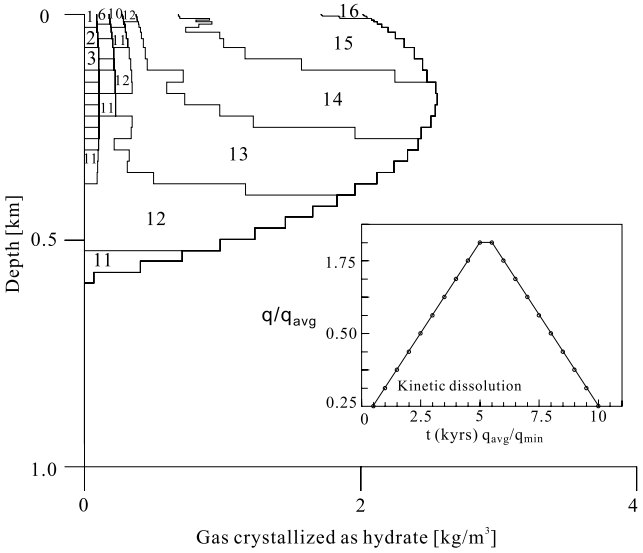

Figure 5. Composition of hydrate crystallized as a function of depth when the gas mass flux, q, increases from $0.25q_{avg}$ in steps of $0.1875q_{avg}$ to $1.93259q_{avg}$ and then ramps down symmetrically, as shown in the insert. The kinetics of crystallization assume $S = 1$ in equation (5). Hydrate bin numbers are shown. Compositions are given in Table 1.

with hydrate in an element is not large. Elements at the base of the stability zone of a hydrate bin will dissolve first. Hydrate in the same bin farther up section will be protected by the increases in X^g produced by deeper dissolution. This is the explanation for the bands of hydrate dissolution in Figure 6. Hydrate can be crystallizing at the same time and in the same element where hydrate is dissolving. The net result is a shuffling of the hydrate from higher to lower compositional bins. By comparing Figure 6 to kinetically controlled calculations in which $S > 1$ (equation (5)), we have found that the dissolution is effectively infinitely fast when $S \sim 100$.

[26] Finally, Figures 7 and 8show what happens when a hydrate mound constructed by a cycle of increasing and decreasing venting rates, as shown in Figure 6, is subjected to an increase in bottom water temperature. We create a numerical mound assuming hydrate dissolution is infinitely fast, as in Figure 6. After ramping the venting rate up and down we keep the venting rate constant at $0.25q_{avg}$, increase the bottom water temperature from 7°C to 12°C, and calculate the consequences of this temperature increase over the next 40 days. The 14 time intervals discretizing this time series are 0.2, 0.4, 0.4, 0.5, 0.5, 1, 1, 2, 2, 2, 5, 5, 5, and 5 days. Figure 7a shows how the bottom water temperature increase propagates into the upper 3 m of sediments. Figures 7b, 7c, and 8 show how this heating affects the vent gas composition, venting rate, and subsurface hydrate composition. The maximum venting rate increase (Figure 7c) caused by the increase in bottom water temperature is 8.3% of the gas flux through the system at the time (in this case, $0.25q_{avg}$). The thermal dissolution of hydrate causes the vent gas mass fraction, X^g, to increase from 0.034 to 0.055 (Figure 7b).

[27] It is important to realize that even for infinitely fast kinetics the increase in venting rate is a percentage of the venting rate at the time. This is because even with fast kinetics the dissolution is still thermodynamically controlled. The dissolution is arrested when the $C_3 + C_4$ mass fraction in the vent gas increases to the point that the vent gas is in equilibrium with as yet undissolved hydrate. This "equilibrium" venting rate increase can be verified from mass balance considerations. Combining equations (7) and (9), the increase in venting rate caused by the dissolution of the mass of hydrate required to bring the vent gas into equilibrium with subsurface hydrate at the new temperature is

$$\frac{q_s}{q_{in}} = 1 + \left(\frac{X_j^{eq-H} - X^g}{X_j^H - X_j^{eq-H}} \right). \tag{14}$$

Here q_{in} is the gas mass flux below the zone of thermal disturbance, and q_s is the mass flux at the sediment water interface. Taking $X_j^H = 0.326$ (the composition of bin 15 hydrate, the wettest hydrate present in the thermally disturbed zone), $X_j^{eq-H} = 0.0558$ (the gas composition in equilibrium with bin 15 hydrate at 12°C), and $X^g = 0.0307$ (the composition of the gas entering the base of the thermally disturbed zone), we find $q_s/q_{in} = 1.0929$. Since we have constrained the kinetics of crystallization so that near the surface $q_{in} = 0.9\ q_{avg}$, we find directly that $\Delta q_s = 0.084\ q_{avg}$, which is the same as that computed value in Figure 7c.

[28] The observed temperature-correlated increases in gas discharge in Figure 1 are clearly much larger than 8.4%. Assuming an initial bottom water temperature of 7°C, the first, ~3 day, temperature increase is at most ~2°C, yet it

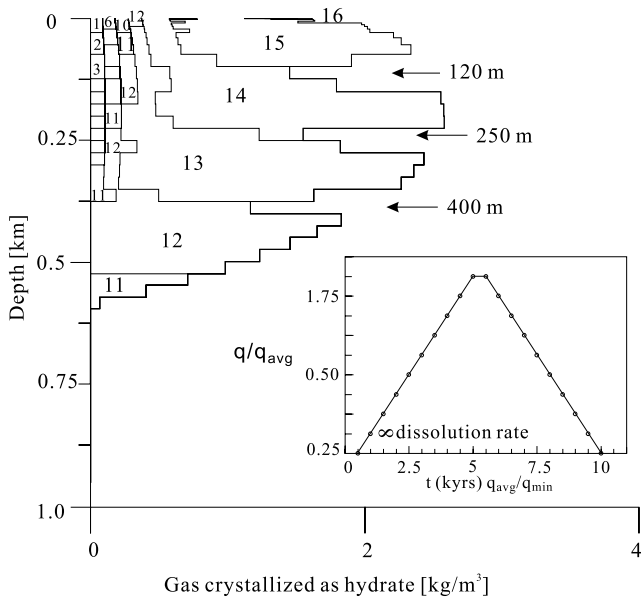

Figure 6. Composition of hydrate crystallized as a function of depth when the gas mass flux increases and then decreases as in Figure 6, but in this case the dissolution kinetics are infinitely fast and the dissolution is stopped only when the composition of the gas stream equilibrates with crystallized hydrate. Hydrate bin numbers are shown. Compositions are given in Table 1.

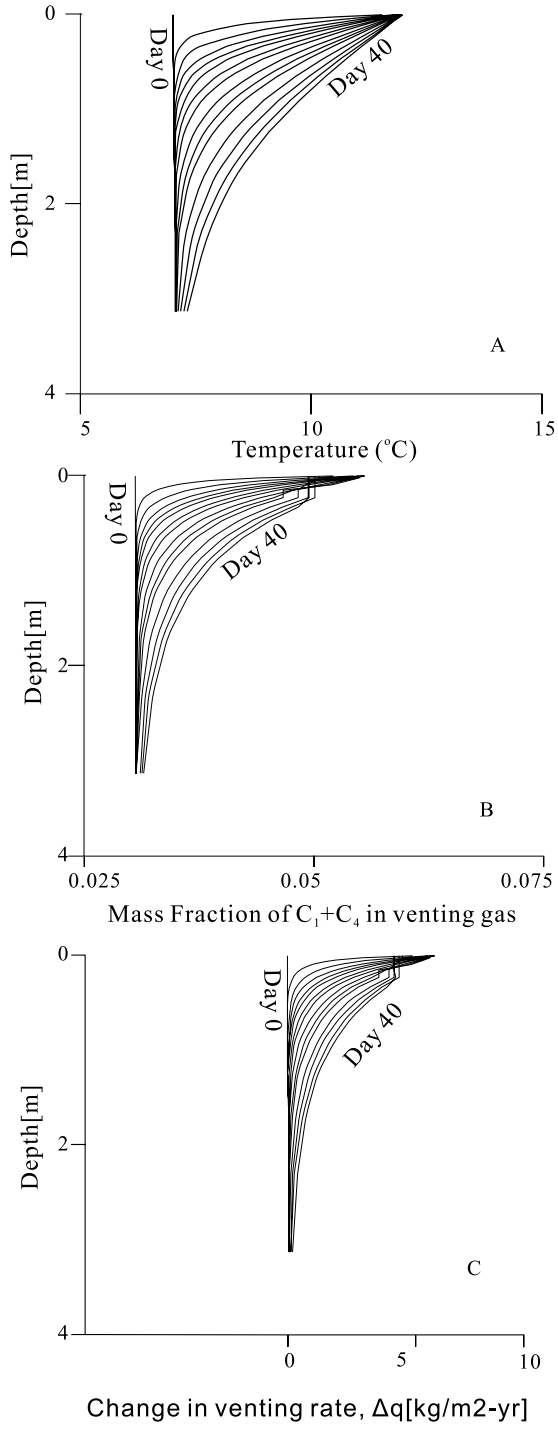

Figure 7. (a) Subsurface temperature for 40 days following an increase in bottom water temperature form 7°C to 12°C. Changes in the upper ~3 m of sediment column are shown. (b) Mass fraction C_3 + C_4 in the vent gas composition associated with the temperature changes in Figure 7a. X^g increases from 0.0304 to 0.0552 by hydrate dissolution. The gas mass fraction drops to 0.0495 when the wettest hydrate bin is depleted. (c) Vent gas mass flux associated with the temperature changes in Figure 7a. The gas flux increases at most 8.3%.

correlates with a 200% increase in venting rate (from 150 to 450 rotations per unit time). Such an increase is possible, but it requires destabilization of more near-surface hydrate than is allowed under thermodynamic equilibrium conditions. For example, if the venting rate is ~20 t yr^{-1} as suggested by *Sassen et al.* [2001b] and 2 vol % hydrate is dissolved to 1 m depth over the 8 m diameter exposure of gas hydrate, the dissolution discharge rate is 15 t yr^{-1}, sufficient to increase the "normal" venting rate by 75%. The dissolution can be large if chemical equilibration can be avoided.

5. Discussion

[29] The above calculations show that decreases in venting rate could cause hydrate dissolution in a hydrate mound and increases in seafloor temperature might affect the rate of discharge at individual gas vents. Both require hydrate dissolution kinetics to be much faster than the crystallization kinetics for significant effects to be produced. Even if the dissolution kinetics are infinitely fast, hydrate dissolution caused by increases in seafloor temperature will increase venting rates by >10% only if the dissolved gas is rapidly removed from the hydrate so that the dissolution reaction is not shut off by reequilibration of the gas stream with adjacent hydrates at the new temperature.

[30] We will not know if there is significant dissolution within a hydrate mound caused by variations in venting rate

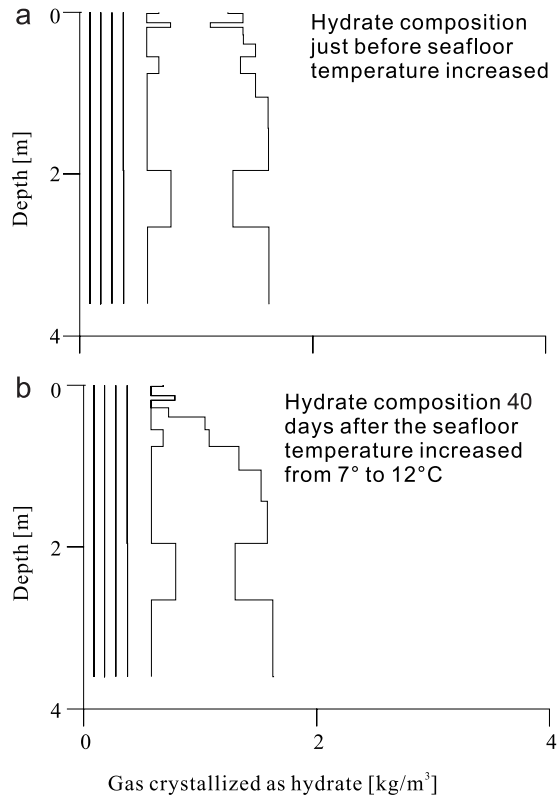

Figure 8. Hydrate distribution in the upper few meters of the subsurface (a) just before and (b) 40 days after the seafloor temperature increases from 7°C to 12°C as shown in Figure 7a. Dissolution kinetics are instantaneous as in Figure 7a.

until one is drilled. Even then it may be difficult to recover unaltered samples for petrographic examination or to image the borehole with sufficient resolution to see the dissolution. Dissolution within the mound could be of interest if the hydrates were to be extracted by solution mining techniques, however, since the dissolution might produce permeable zones in the mound.

[31] There is substantial circumstantial evidence for very rapid dissolution of near-surface hydrate. Rapid dissolution is suggested by reports of mounds disappearing between submersible visits [*MacDonald et al.*, 1994, 2003]. A Savonius rotor, not the one whose data is shown in Figure 1, measuring the venting rate of a bubble stream at Bush Hill plugged with hydrate in May 2002. When the robot arm of Johnson-Sea-Link II submersible was taking the rotor to the submersible basket, hydrate clumps centimeters in diameter were observed to disappear within seconds. This suggests that hydrate can be decomposed simply by raising the hydrate temperature and that the decomposition is rapid on the timescale of hours or fractions of a day.

[32] *Carson et al.* [2003] report strong evidence for very rapid hydrate dissolution in an instrumented hole on Hydrate Ridge on the Cascadia margin at Ocean Drilling Program (ODP) Site 892B. A partial hydrate blockage of the flow path in the instrument occurred on day 26 of their experiment. The flow became increasingly restricted, and pore pressures in excess of hydrostatic rose to the detection limit of their instruments by day 66. On day 127 the borehole pressure dropped rapidly for 27 days at which time it was ~35 kPa under pressured. The explanation offered by Carson et al. is that the hydrate that had blocked the water flow had dissociated and dissolved. This inference is substantiated by a simultaneous drop in salinity recorded by their OsmoSamplers.

[33] Rapid dissolution of hydrate is plausible. Hydrate is very porous (10–40 vol % pores [*Kuhs et al.*, 2000; *Klapproth et al.*, 2003]). The high porosity suggests that the permeability is also high since permeability and porosity are often correlated. Thus dissolution gas could buoyantly rise rapidly from the hydrate, drawing in water or unsaturated gas that would not inhibit the decomposition.

[34] The vent rate monitoring in Figure 1 is not without its complications and shows features not yet discussed that warrant mention. Positive excursions in the venting rate correlate with increases in bottom water temperature, but this response becomes less strong with time. The largest increase in venting rate occurred at ~2 days and is correlated with a strong spike in bottom water temperature. A broad increase in bottom water temperature starting at ~15 days correlates with a broad but smaller increase in gas emission rate. There is no increase in gas venting rate at the strongest spike in bottom water temperature at ~35 days. As discussed by *Roberts* [2001], this is probably mostly due to the plugging of the rotor with hydrate. However, it could also be partly due to the depletion of compositionally unstable hydrates in the near surface by the first two thermal excursions. If so, it would be a chemically expected decrease and would constitute a confirmation of the model that we have constructed.

[35] There are several important limitations on the applicability of the current model. As q_{avg} increases above q_{min}, heat advection by the gas stream and the heat released by crystallization of hydrate will change the subsurface temperature profile and invalidate our assumption that the subsurface temperature gradient is conductive. Heat flow is perturbed significantly by advection when the Peclet number, *Pe*, exceeds ~2 [*Bredehoeft and Popadopulos*, 1965]. The minimum gas mass flux through the Bush Hill mound is 1.6 kg m^{-2} yr^{-1}. Taking thermal conductivity K [W m^{-1} °C^{-1}] = 1.5, gas heat capacity c_g [J kg^{-1} °C^{-1}] = 2650, and Δz [m] = 600, $Pe = qc_g\ \Delta z/K = 0.054$. Thus the thermal gradient will be perturbed significantly by the gas flow when $q_{\mathrm{avg}} > 37q_{\mathrm{min}}$. Latent heat of crystallization will become important when the rate of its release becomes an appreciable fraction of the normal heat flow. Since the temperature gradient in the Bush Hill area is ~20°C km^{-1}, the heat flow there is j_H [mW m^{-2}]~30. The latent heat of hydrate crystallization of hydrate is L [J g^{-1}]~421 [*Rueff et al.*, 1988]. Thus the added heat flux due to hydrate crystallization at the minimum gas flux is $j_{\mathrm{hyd}} = 0.09\ q_{\mathrm{min}}L = 2$ mW m^{-2}.

[36] When the gas flux exceeds $7.5q_{\mathrm{min}}$, the heat flow added by hydrate crystallization will equal half the normal heat flow at Bush Hill, and this could increase the geothermal gradient from 20 to 30°C km^{-1} or more.

[37] These limitations are not of importance to the very near surface dissolution of hydrate caused by bottom water temperature increases that we address in this paper. It does not matter how the mix of near-surface hydrate compositions is established, and the temperature gradient near the surface is not an important parameter so long as it is not so steep that no significant hydrate can accumulate within a few meters of the surface. This is not the case. However, heat advection by the gas stream and the latent heat of hydrate crystallization must clearly be taken into account if we want to realistically simulate hydrate accumulation in the Bush Hill mound when the gas vents through channels that form a relatively small fraction of the plan section of the mound. Gas venting is almost certainly channeled in this fashion at Bush Hill because venting seems to be occurring at very discrete locations on the mound [*De Beukelaer et al.*, 2003]. We do not know the distribution of bubble vents on the mound, and diffuse leakage could also be occurring. Addressing the evolution of the mound and its channels theoretically will require two-dimensional heat and gas flow modeling in which heat advection by the gas and latent heat of hydrate crystallization and dissolution are taken into account.

[38] Another aspect of our model should be mentioned. The kinetics of dissolution and crystallization are not symmetric. The crystallization kinetics are driven by the difference between the gas stream mass fraction X^g and a fictive equilibrium gas mass fraction X_j^{g-eq} that is negative at shallow depths [*Chen and Cathles*, 2003, equation (1) and Figure 3], whereas the dissolution kinetics are driven by the difference between the gas composition and that which would be in equilibrium with hydrate in bin j, $X_j^{g-\mathrm{eq}H}$ (equation (5)). Since $X_j^{g-\mathrm{eq}H}$ is never negative, the kinetics of dissolution can be significantly slower than the kinetics of dissolution (for the same rate constant) just because of the formalisms we adapt. Since we find that the dissolution kinetics are probably very much faster than the crystallization kinetics and apply the model only for infinitely fast dissolution kinetics in this paper, this asymmetry or unequal kinetic treatment is not important to the current discussion.

[39] Finally, we would emphasize that the crystallization and dissolution rate constants are empirically calibrated to the observed operation of gas venting on the Bush Hill mound. We consider this unavoidable because of the many factors that would be required to build a kinetic model of hydrate crystallization in a natural system from first principals. The complications are discussed by *Chen and Cathles* [2003]. Models can be useful in identifying the parameters required for a natural system to operate as observed, and we hope this will be the case with the inferences we have made in this paper regarding hydrate crystallization and dissolution rate constants.

6. Conclusions

[40] We develop a compositional kinetic model of hydrate crystallization and dissolution and use it to examine how hydrates crystallize and dissolve in the Bush Hill hydrate mound as the rate of gas venting changes and to predict how near-surface hydrate may dissolve when bottom water temperature increases. We show that subsurface hydrate dissolution is significant only if the kinetics of hydrate dissolution (as characterized in our model) are fast with respect to hydrate crystallization. We show that for infinitely fast dissolution kinetics, increases in bottom water temperature could increase gas venting rates by $\sim$10% by dissolving hydrates in the upper few meters of a hydrate mound. This limitation is imposed by the fact that hydrate dissolution will bring the gas into thermodynamic equilibrium with adjacent hydrate at the new temperature conditions and stop the dissolution reaction. Since much larger rates of dissolution seem to occur, it must be possible to circumvent this thermodynamic shutoff, and we suggest that this occurs because unsaturated gas or water is drawn in as the dissolution gas escapes.

[41] If hydrate dissolution is as rapid as the dissolution of near-surface hydrate suggests, our model predicts that hydrate dissolution should occur in the interior of the Bush Hill mound when the gas venting rate drops. The mound interior should show evidence of hydrate dissolution. This, as well as the acquisition of quality time series of bottom surface temperature and the rate and composition of gas vents, could provide tests of the model.

[42] **Acknowledgments.** Cathles and Chen are grateful to H. Roberts and the Minerals Management Service for encouragement of the work, especially for an invitation to participate on the submersible investigation of the Gulf of Mexico in May 2002. The hydrate dissolution process described above was observed in this cruise. Chen acknowledges the support of the NSFC (project 40072044) and the Chinese Academy of Sciences (Projects MSGLCASO3-1, KZCX3-SW-219, and KZCX2-SW-309). Funds from the corporate sponsors of the Global Basins Research Network supported Chen in the United States. The authors are grateful to Ian MacDonald and Wenyue Xu and an anonymous editor for exceptionally helpful reviews that led to a substantially modified and improved manuscript. Wenyue Xu suggested the potential impact of the latent heat of hydrate crystallization, which we had mistakenly assumed to be negligible.

References

Baker, A. S., and D. W. Pepper (1991), *Finite Elements 1–2–3*, 341 pp., McGraw-Hill, New York.

Bredehoeft, J. D., and I. S. Popadopulos (1965), Rates of vertical ground water movement estimated from the Earth's thermal profile, *Water Resour. Res.*, *1*, 325–328.

Carson, B., M. Kastner, D. Bartlett, J. Jaeger, H. Jannasch, and Y. Weinstein (2003), Implications of carbon flux from the Cascadia accretionary prism: Results from long-term, in situ measurements at ODP Site 892B, *Mar. Geol.*, *198*, 159–180.

Chen, D. F., and L. M. Cathles III (2003), A kinetic model for the pattern and amounts of hydrate precipitated from a gas steam: Application to the Bush Hill vent site, Green Canyon Block 185, Gulf of Mexico, *J. Geophys. Res.*, *108*(B1), 2058, doi:10.1029/2001JB001597.

Chen, D. F., L. M. Cathles, and H. H. Roberts (2004), The chemical signatures of variable gas venting at hydrate sites, *Mar. Pet. Geol.*, *21*, 317–326.

De Beukelaer, S. M., I. R. MacDOnald, N. L. Guinnasso Jr., and J. A. Murray (2003), Distinct side-scan sonar, RADARSAT SAR, and acoustic profiler signatures of gas and oil seeps on the Gulf of Mexico slope, *Geo Mar Lett.*, *23*, 177–186.

Dickens, G. R., and M. S. Quinby-Hunt (1997), Methane hydrate stability in pore water: A simple theoretical approach for geophysical applications, *J. Geophys. Res.*, *102*, 773–783.

Hyndman, R. D., and E. E. Davis (1992), A mechanism for the formation of methane hydrate and seafloor bottom simulating reflectors by vertical fluid expulsion, *J. Geophys. Res.*, *97*, 7025–7041.

Klapproth, A., E. Goreshnik, D. Staykova, H. Klein, and W. F. Kuhs (2003), Structural studies of gas hydrates, *Can. J. Phys.*, *81*(1–2), 503–518.

Kuhs, W. F., A. Klapproth, F. Gotthardt, K. Techmer, and T. Heinrichs (2000), The formation of meso- and macroporous gas hydrates, *Geophys. Res. Lett.*, *27*, 2929–2932.

Kvenvolden, K. A., and T. D. Lorenson (2001), The global occurrence of natural gas hydrates, in *Natural Gas Hydrates: Occurrence*, *Distribution, and Detection*, *Geophys. Monogr. Ser.*, vol. 124, edited by C. K. Paull and W. P. Dillon, pp. 3–18, AGU, Washington, D. C.

Luo, M., J. R. Wood, and L. M. Cathles (1994), Prediction of thermal conductivity in reservoir rocks using fabric theory, *J. Appl. Geophys.*, *32*(4), 321–334.

MacDonald, I. R., N. L. Guinasso Jr., R. Sassen, J. M. Brooks, L. Lee, and K. T. Scott (1994), Gas hydrate that breaches the seafloor on the continental slope of the Gulf of Mexico, *Geology*, *22*(8), 699–702.

MacDonald, I. R., W. W. Sager, and M. B. Peccini (2003), Gas hydrate and chemosynthetic biota in mounded bathymetry at mid-slope hydrocarbon seeps: northern Gulf of Mexico, *Mar. Geol.*, *198*, 133–158.

Rempel, A. W., and B. A. Buffett (1997), Formation and accumulation of gas hydrate in porous media, *J. Geophys. Res.*, *102*, 10,151–10,164.

Revil, A., and L. M. Cathles (2002), Fluid transport by solitary waves along growing faults: A field example from the South Eugene Island Basin, Gulf of Mexico, *Earth Planet. Sci. Lett.*, *202*(2), 321–335.

Roberts, H. H. (2001), Fluid and gas expulsion on the northern Gulf of Mexico continental slope: Mud-prone to mineral-prone responses, in *Natural Gas Hydrates: Occurrence*, *Distribution, and Detection*, *Geophys. Monogr. Ser.*, vol. 124, edited by C. K. Paull and W. P. Dillon, pp. 145–161, AGU, Washington, D. C.

Roberts, H. H., and R. S. Carney (1997), Evidence of episodic fluid, gas, and sediment venting on the northern Gulf of Mexico continental slope, *Econ. Geol.*, *92*(7–8), 863–879.

Roberts, H. H., W. J. Wiseman, J. Hooper, and G. D. Humphrey (1999), Surficial gas hydrates of the Louisiana Continental slope-initial results of direct observations and in situ data collection, paper presented at Offshore Technology Conference, Houston, Tex.

Rueff, R. M., E. D. Sloan, and V. F. Yesavage (1988), Heat capacity and heat of dissociation of methane hydrates, *Am. Inst. Chem. Eng.*, *34*, 1468–1476.

Sassen, R., S. L. Losh, L. M. Cathles, H. H. Roberts, J. K. Whelan, A. V. Milkov, S. T. Sweet, and D. A. DeFreitas (2001a), Massive vein-filling gas hydrate: Relation to ongoing gas migration from the deep subsurface in the Gulf of Mexico, *Mar. Pet. Geol.*, *18*, 551–560.

Sassen, R., S. T. Sweet, A. V. Milkov, D. A. DeFreitas, M. C. Kennicutt, and H. H. Roberts (2001b), Stability of thermogenic gas hydrate in the Gulf of Mexico: Constraints on models of climate change, in *Natural Gas Hydrates: Occurrence*, *Distribution, and Detection*, edited by C. K. Paull and W. P. Dillon, pp. 131–143, AGU, Washington, D. C.

Sloan, E. D. (1998), *Clathrate Hydrates of Natural Gases*, 2nd ed., 628 pp., Marcel Dekker, New York.

Xu, W., and C. Ruppel (1999), Predicting the occurrence, distribution, and evolution of methane gas hydrate in porous marine sediments, *J. Geophys. Res.*, *104*, 5081–5096.

L. M. Cathles, Department of Earth and Atmospheric Sciences, Cornell University, Snee Hall, Ithaca, NY 14853-1504, USA. (cathles@geology.cornell.edu)

D. Chen, Key Laboratory of Marginal Sea Geology, Guangzhou Institute of Geochemistry, Chinese Academy of Sciences, Wushan, Guangzhou, Guangdong 510640, China.